From quasiperiodicity to toroidal chaos: Analogy between the Curry-Yorke map and the van der Pol system

Christophe Letellier,[1] Valérie Messager,[1] and Robert Gilmore[1,2]
[1]*CORIA UMR 6614-Université de Rouen, BP 12, F-76801 Saint-Etienne du Rouvray cedex, France*
[2]*Physics Department, Drexel University, Philadelphia, Pennsylvania 19104, USA*
(Received 24 July 2007; revised manuscript received 12 December 2007; published 7 April 2008)

The van der Pol attractor exhibits a wide variety of behavior depending on the control parameter values: limit cycles, quasiperiodic motion on a torus, mode locking, period doubling, banded chaos, boundary crises, torus wrinkling, breakup of a torus, and toroidal chaos. The organization of these phenomena with respect to each other is well described by studying a partition of the control parameter plane of the Curry-Yorke map.

DOI: 10.1103/PhysRevE.77.046203 PACS number(s): 05.45.−a

I. INTRODUCTION

The periodically driven van der Pol oscillator [1,2] can exhibit a large variety of complicated behavior, ranging from simple limit cycles, mode-locked limit cycles, quasiperiodic motion, banded chaotic attractors, and chaotic toroidal attractors.

The transition from quasiperiodic motion on a torus to chaotic behavior occurs by breakup of the torus. The breakup of the torus manifests itself in several different ways. One path to chaos involves a period-doubling cascade that occurs within a mode-locked tongue. This leads to a banded chaotic attractor, which evolves into a wrinkled fractal toroidal attractor following one or more boundary crises. Another path to a chaotic toroidal attractor involves wrinkling of the torus until a structurally stable heteroclinic invariant set is created. When this occurs inside a mode-locked tongue the heteroclinic invariant set is dynamically unstable and essentially invisible until the edge of the tongue is crossed. Then the mode-locked behavior suddenly disappears and is replaced by a chaotic toroidal attractor in a "hard" transition to chaos. This wrinkling can also take place outside an Arnol'd tongue. In this case the transition to chaos is "soft."

We investigate the sequence of transitions among these types of behaviors through intersections of the attracting set with a Poincaré surface of section and bifurcation diagrams of these attracting sets. This is most easily done by studying the properties of return maps onto the Poincaré section. Since it is not possible to compute an analytic form for the return map of the van der Pol oscillator onto a Poincaré surface of section, we use as a surrogate one of the standard well-known maps, the Curry-Yorke map [3]. Both the periodically driven van der Pol oscillator and the Curry Yorke map satisfy the conditions of the Afraimovich-Shilnikov theorem [4–6], which describes the spectrum of possible routes from quasiperiodicity through torus breakup to toroidal chaos. Other maps, such as the Zaslavsky map [7,8], can be used. We have used the Curry-Yorke map because it is among the simplest invertible maps $\mathbb{R}^2 \to \mathbb{R}^2$ that depend on two control parameters, so that is it possible to follow nontrivial paths through the control parameter plane. One control parameter is insufficient to illustrate this spectrum of behaviors, and two are necessary and also sufficient to exhibit all the phenomena that are observed [4–6], while three or more (as in the van der Pol system itself or the Zaslavsky map) simply complicate this study.

In Sec. II we introduce a version of the van der Pol dynamical system. The behavior of this system is studied through a set of bifurcation diagrams in the Poincaré section defined by $\omega t = 0 \bmod 2\pi$. Several types of behavior are illustrated for this system. The organization of this behavior is clarified in Sec. III. There we introduce the Curry-Yorke map, exhibit the decomposition of its control parameter space into various important regions (cf. Fig. 5), and follow two different paths through the control parameter space. Along each we describe the changes that are encountered by showing phase-space portraits that occur along these paths. The phase-space portraits of the Curry-Yorke map are to be compared with intersections of the van der Pol attractor with a Poincaré section. By inspection of the decomposition of the control parameter space it is possible to devise paths for scenarios involving transitions among different types of behavior, including limit cycle, quasiperiodic, mode-locked, banded chaos, and toroidal chaos behaviors. Many of the phenomena exhibited in the transition to chaos are consequences of the Afraimovich-Shilnikov theorem, which we summarize in Sec. IV. This theorem is local and does not describe phenomena related to coexisting basins of attraction. We point out these additional consequences and show similarities in the behavior of the van der Pol flow and the Curry-Yorke map in this section. We summarize our findings in the Conclusion.

II. van der POL SYSTEM

A. Equations

Ueda and co-workers [1,2] were among the first to study the chaotic behavior generated by the van der Pol dynamical system. They studied the following equation:

$$\ddot{x} - \mu(1 - \gamma x^2)\dot{x} + x^3 = B\cos(\omega t). \tag{1}$$

This can be expressed as a nonautonomous dynamical system in the form

$$\dot{x} = y,$$

$$\dot{y} = \mu(1 - \gamma x^2)y - x^3 + B\cos(\omega t). \quad (2)$$

The phase space for this dynamical system is $D^2 \times S^1$, where $D^2 \subset \mathbb{R}^2$ is a disk of finite diameter in $\mathbb{R}^2$ and S^1 describes motion around the torus in terms of an angle $\phi = \omega t \bmod 2\pi$. The behavior exhibited by this dynamical system depends on the control parameters (μ, γ, B, ω). This set of equations has a twofold internal symmetry under $(x,y,t) \rightarrow (-x,-y,t+\frac{1}{2}T)$, where $\omega T = 2\pi$. This symmetry has the following consequence. If symmetry-related initial conditions (x,y,t) and $(-x,-y,t+\frac{1}{2}T)$ are on a periodic orbit, either they are on the same orbit (called a symmetric orbit) or else they are on two different orbits that form a symmetry-related pair of orbits. A symmetric orbit cannot undergo a period-doubling bifurcation [9]. As a result, any orbit that undergoes a period-doubling bifurcation is not symmetric and has a symmetry-related partner that also undergoes a period-doubling bifurcation.

The equation can also be rewritten as a set of four first-order autonomous ordinary differential equations

$$\dot{x} = y, \quad \dot{u} = v,$$

$$\dot{y} = \mu(1 - \gamma x^2)y - x^3 + u, \quad \dot{v} = -\omega^2 u. \quad (3)$$

This version of Eq. (1) depends on the control parameters (μ, γ, ω) and initial conditions $(u,v) = (B,0)$. We point out here that when the van der Pol system is expressed as an autonomous dynamical system, the parameter B clearly appears as an initial condition and not as a bifurcation parameter. This explains why "bifurcation diagrams" parametrized in terms of B are usually so difficult to interpret [10].

The van der Pol system (3) is equivariant under an inversion symmetry $(x,y,u,v) \rightarrow (-x,-y,-u,-v)$. The twofold symmetry will present a slight complication in comparing the behavior in the return map on a Poincaré section with the behavior of the Curry-Yorke map.

This system is often used as a benchmark model for torus breakdown and for investigating some bifurcation diagrams with mode-locking and period-doubling cascades [11–14].

B. Bifurcation behavior and phase portraits

In the absence of periodic forcing $[B=0$ or $(u,v)=(0,0)]$ the origin $(x,y)=(0,0)$ is a fixed point. As μ becomes positive, a Hopf bifurcation occurs that creates a stable limit cycle as the fixed point at the origin becomes unstable.

When the forcing is turned on $(B \neq 0)$, the stable fixed point at the origin of $\mathbb{R}^4$ for $\mu < 0$ becomes a stable period-1 orbit. As μ increases above zero, this period-1 orbit loses its stability, giving rise to quasiperiodic motion on a torus that surrounds the unstable limit cycle. Another way to view this is that the unstable fixed point at the origin and the stable limit cycle that exist in the x-y plane for $\mu > 0$ and $B=0$ evolve, for $B \neq 0$, to an unstable limit cycle and a torus on which the phase space trajectory moves in $D^2 \times S^1$. While the torus exists, the motion on it alternates between quasiperiodic and periodic (mode-locked) motion as the control parameters vary.

Figure 1 shows a bifurcation diagram for Eq. (2). The diagram is constructed by recording the value of y at each intersection with a Poincaré section, defined by $\omega t = 0 \bmod 2\pi$. Sweeps that were made for γ ascending and γ descending show hysteresis because of the multistability exhibited by this system. For each change in the value of γ the initial conditions used for the new iteration were the final values for the previous.

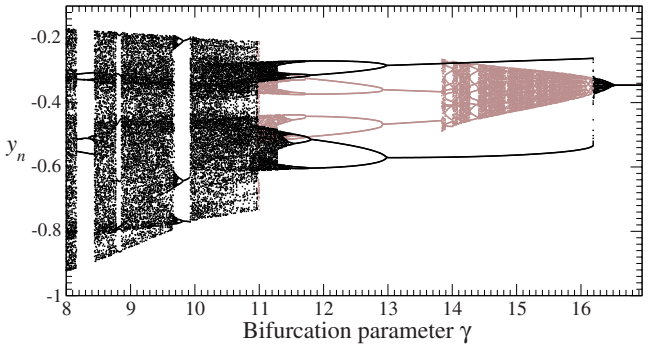

FIG. 1. (Color online) Bifurcation diagram versus γ for the van der Pol system studied by Ueda. Dark, γ increasing; light, γ decreasing. Hysteresis reveals multistability. Other parameter values: $\mu=0.2$, $B=0.35$, and $\omega=1.018$.

On the ascending sweep (black) there is a mixture of chaotic and periodic behavior up to $\gamma=11.0$. From $\gamma=11.0$ to $\gamma=11.3$ there is an attractor with two bands. The intersections of these attractors with a Poincaré section is shown in Fig. 2. For $\gamma=10.97$, just below the merging crisis, the attractor exhibits toroidal chaotic behavior [Fig. 2(a)]. For $\gamma=11.03$, just above this crisis, the bifurcation diagram shows an attractor with two bands. The bands are formed after accumulation of a period-doubling cascade with γ decreasing through 11.3. The period-doubling cascade shown in the bifurcation diagram occurs on one of a pair of symmetry-related period-2 orbits. Each creates an attractor with two bands. The two-band attractors associated with each of the symmetry-related orbits are shown in Fig. 2(b). A period-2 orbit appears at $\gamma=13.0$ and coexists with other attractors until it is destroyed in an inverse saddle-node bifurcation at $\gamma=16.2$. The attractor shown in the bifurcation diagram is quasiperiodic from $\gamma=16.2$ to $\gamma=16.4$, where an inverse Hopf bifurcation destroys quasiperiodicity and replaces it with a stable period-1 orbit.

In the bifurcation diagram the period-2 orbits are represented by two points for any value of γ and quasiperiodic behavior appears as a small range of intersections around $y_n=-0.35$. In Fig. 3 we show phase portraits of the attractors encountered along the ascending path. Figure 3(a) shows the period-2 orbit that is represented in the bifurcation diagram at $\gamma=13.026$ (plotted in black) as well as its symmetry-related partner, plotted in red. This partner orbit is not seen in the bifurcation diagram. Both orbits are stable and each is associated with it an unstable period-2 saddle. The phase portrait of the quasiperiodic trajectory at $\gamma=16.2$ is shown in Fig. 3(b). This shrinks down to a roughly circular period-1 orbit (not shown) for $\gamma > 16.4$.

On the descending sweep some differences are apparent. For $\gamma=17$ there is a stable period-1 orbit. A Hopf bifurcation

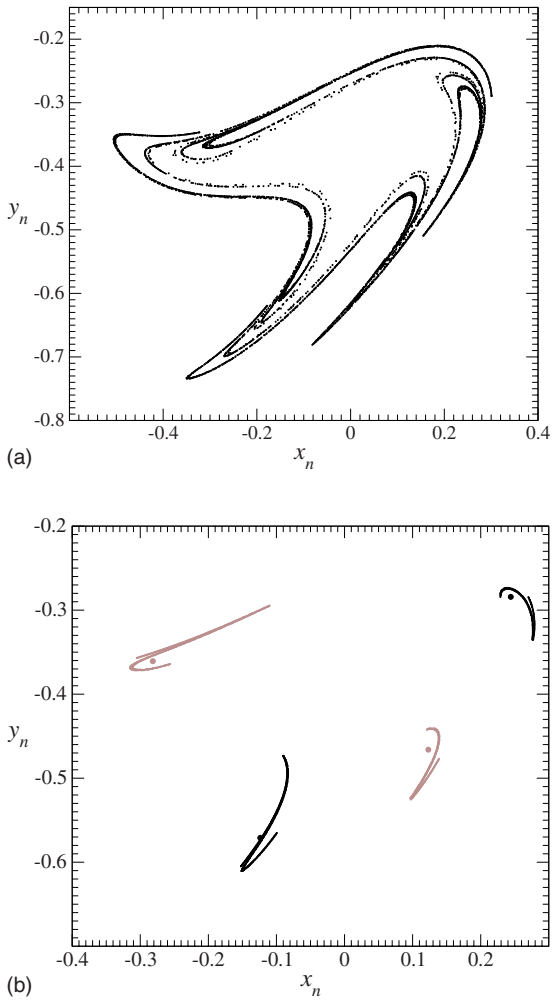

FIG. 2. (Color online) Chaotic behavior of the van der Pol system on a Poincaré section. (a) Toroidal chaotic behavior. (b) Banded chaotic behavior. The two pairs of period-2 points shown correspond to period-2 stable limit cycles at $\gamma=13.026$ (dark trace). A boundary crisis separates banded chaos from toroidal chaos. (a) $\gamma=10.97$ and (b) $\gamma=11.03$. Other parameter values: $\mu=0.2$, $B=0.35$, and $\omega=1.018$.

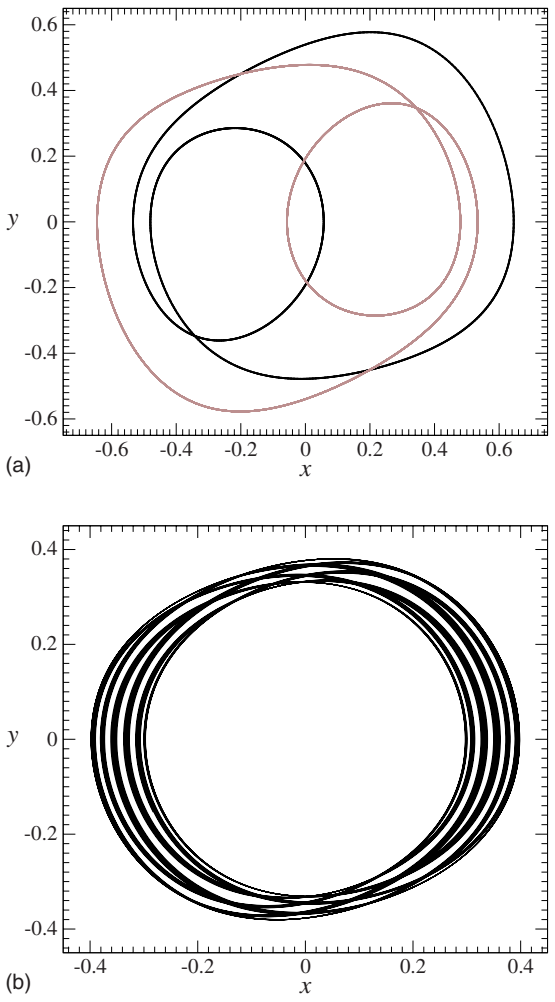

FIG. 3. (Color online) Phase-space plots of solutions to the van der Pol system. (a) Two coexisting stable period-2 limit cycles ($\gamma=13.026$). They are symmetry related, one being mapped to the other under the inversion symmetry. Only one is indicated in the bifurcation diagram of Fig. 1 on the ascending path. (b) Quasiperiodic solution ($\gamma=16.2$). Other parameter values: $\mu=0.2$, $B=0.35$, and $\omega=1.018$.

at $\gamma=16.4$ changes the stability of this orbit and creates a stable quasiperiodic attractor. This exists (alternating with mode locking) and is followed in the bifurcation diagram down to $\gamma=13.9$ where a saddle-node bifurcation on the invariant torus creates a stable period-2 orbit that is not related to the larger period-2 orbit followed along the path of γ increasing. The period-2 orbit undergoes a period-doubling cascade and eventually produces a two-band attractor at $\gamma=11.3$. This is different from the pair of two-band attractors seen in the Poincaré section shown in Fig. 2(b). At $\gamma=11.3$ a crisis creates a toroidal chaotic attractor. Hysteresis is apparent in the range $11.0<\gamma<16.2$. In the range $11.0<\gamma<13.9$ at least four basins of attraction coexist. Two surround each of the symmetry-related period-2 orbits, one of which is tracked for γ increasing, and two surround each of the symmetry-related pair on the invariant torus, one of which is tracked for γ decreasing. These two pairs of symmetry-related orbits undergo period doubling bifurcations at values of γ that are not the same, despite appearances in Fig. 1.

Toroidal chaos can be reached without going through the period-doubling cascade and the banded attractor phase. This is shown in Fig. 4. As γ increases above 9.1, it enters a period-2 mode-locked tongue. A period doubling bifurcation occurs at $\gamma=9.3$, followed by a period-halving bifurcation at $\gamma=11.8$, a brief interval of quasiperiodicity around $\gamma=15.9$, and a stable period-1 limit cycle for $\gamma>16.0$. The initiation and reversal of period-doubling cascades is a common feature of nonlinear oscillators and is commonly referred to as "period bubbling" [11,15–17]. On decreasing through $\gamma=9.1$ there is a "hard" transition to chaos. The "hard" transition is one of the three routes to toroidal chaos predicted by the Afraimovich-Shilnikov theorem [4–6].

It should be emphasized that the van der Pol oscillator supports coexisting basins of attraction [10,18], as shown in Figs. 1–3.

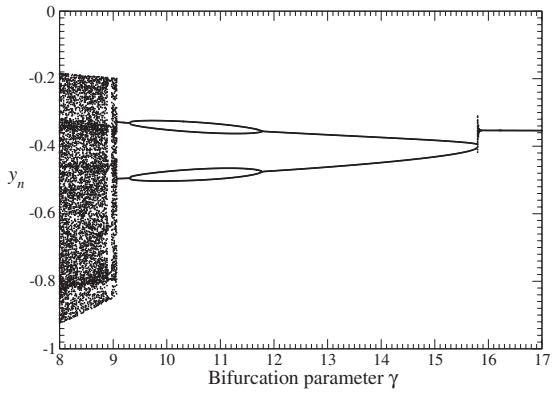

FIG. 4. Bifurcation diagram versus parameter γ for the van der Pol system. For γ decreasing the period-doubling cascade begins and is reversed, followed by a sudden ("hard") transition to toroidal chaos. Other parameter values: $\mu=0.2$, $B=0.35$, and $\omega=1.014$.

III. CURRY-YORKE MAP

The rich behavior seen in the van der Pol dynamical system corresponds closely to the rich behavior exhibited by the Curry-Yorke map. The principal difference between the two is that one is a flow and the other is a map. We use this map as a model for the return flow onto a Poincaré section. A second difference is that the flow exhibits a twofold symmetry in the phase space while the map does not.

A. Map

A homeomorphism on $\mathbb{R}^2$ is a function that is continuous and has a continuous inverse. The mapping Ψ proposed by Curry and Yorke is the composition of two simple homeomorphisms Ψ_1 and Ψ_2. The homeomorphism Ψ_1 is defined in polar coordinates by

$$\Psi_1 \equiv \begin{vmatrix} \rho_{n+1} = \epsilon \ln(1+\rho_n), \\ \theta_{n+1} = \theta_n + \theta_0, \end{vmatrix} \tag{4}$$

where $\epsilon \geq 0$ and θ_0 are control parameters to be chosen. The homeomorphism Ψ_2 is defined in Cartesian coordinates by

$$\Psi_2 \equiv \begin{vmatrix} x_{n+1} = x_n, \\ y_{n+1} = x_n^2 + y_n. \end{vmatrix} \tag{5}$$

The Curry-Yorke map is the composition of these two maps: $\Psi = \Psi_2 \circ \Psi_1$.

This map can be expressed in simpler form in Cartesian coordinates as follows:

$$\begin{bmatrix} x \\ y \end{bmatrix}_{n+1} = \frac{\epsilon}{\rho'} \ln(1+\rho') \begin{bmatrix} \cos\theta_0 & -\sin\theta_0 \\ \sin\theta_0 & \cos\theta_0 \end{bmatrix} \begin{bmatrix} x \\ y+x^2 \end{bmatrix}_n, \tag{6}$$

where $\rho'^2 = x^2 + (y+x^2)^2$.

For all values of the control parameters there is a period-1 orbit (fixed point) at the origin. This fixed point is stable for $\epsilon < \epsilon_1 = 1$ and unstable for $\epsilon > 1$. The origin becomes an unstable focus for $\epsilon > \epsilon_1$ via a Hopf bifurcation. Immediately after the Hopf bifurcation the iterates of an arbitrary initial condition follow a roughly circular quasiperiodic trajectory after the transients have died out. The radius ρ_s of this trajectory is approximated by $\rho_s = \epsilon \ln(1+\rho_s)$. The radius grows linearly with the difference $\epsilon - \epsilon_1$ like $\rho_s \simeq 2(\epsilon - \epsilon_1)/\epsilon$ for small $\epsilon - \epsilon_1$.

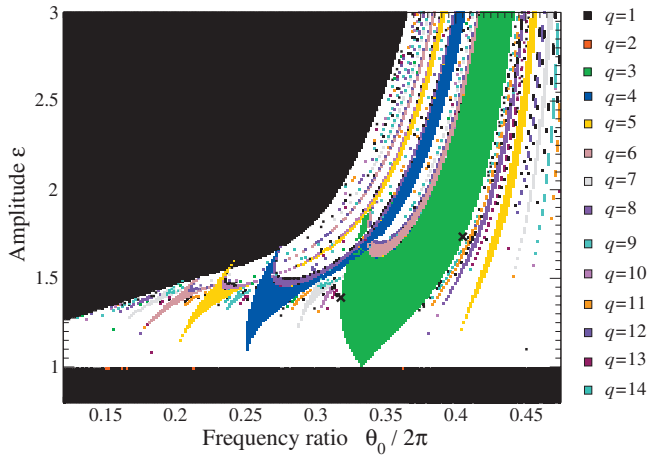

FIG. 5. (Color) Parameter space for the Curry-Yorke map. Arnol'd tongues associated with mode locking are attached to the $\theta_0/2\pi$ axis at p/q and are clearly visible for $p=1$ and $q=3,4,5,6$. Tongues are generally three sided, bounded by saddle-node bifurcation curves along their outer edges that are joined at a vertex on the line $\epsilon=\epsilon_1$ and by the beginnings of period-doubling cascades opposite the vertex. Intersections of the heteroclinic connection curve (Sec. IV) with the saddle node edges of the 1/3 tongue are shown with an x.

Another stable period-1 orbit (and partner saddle) is created in a saddle-node bifurcation for sufficiently large values of ϵ. Its location is determined by fixing θ_0 and looking for a real doubly degenerate solution for the fixed-point equation arising from the first return map, Eq. (6). This defines a curve $\epsilon_2 = f(\theta_0)$ in the control parameter plane. Above this curve there is only one stable attractor of period 1.

B. Control parameter space

Figure 5 provides an overview of the dynamical behavior over an important part of the control parameter space. The figure shows that the parameter space is divided into three important regions: two boundary regions defined by $\epsilon < \epsilon_1$ and $\epsilon > \epsilon_2$ in which only one stable period-1 orbit is observed and an intermediate region showing very complicated behavior. This behavior includes quasiperiodic motion, mode-locked periodic motion, and chaotic motion. The chaotic behavior can be either banded or toroidal. Multistability occurs in this region of the control parameter plane. The partition of the control plane was created by scanning θ_0 from left to right and, for a fixed value of θ_0, scanning ϵ from below ϵ_1 to above ϵ_2, using final values of the previous scan as initial conditions for the next.

It is a simple matter to distinguish periodic from quasiperiodic behavior. In the former case the limit

$$\frac{1}{2\pi} \lim_{n\to\infty} \frac{\theta_n}{n} = (\text{rotation number}) \tag{7}$$

is a rational fraction p/q, where p and q are relatively prime integers. This signifies that the trajectory goes around the

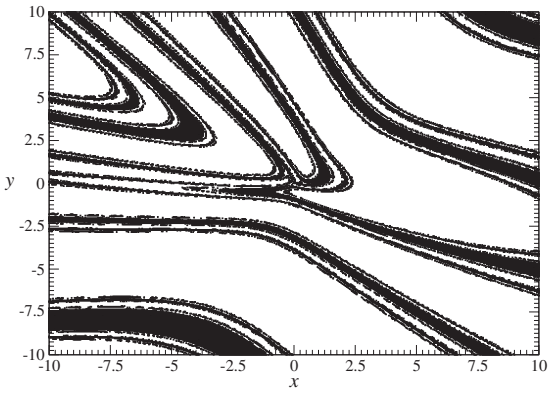

FIG. 6. Multistability in the Curry-Yorke map. Coexisting intertwined basins of attraction of the stable period-3 (black) and period-4 (white) orbits for control parameters $(\epsilon,\theta_0)=(1.7,2.1)$ in the intersection of the period-3 and period-4 windows.

meridian (short circle in the Poincaré surface) of the torus p times and the longitude (long circle) of the torus q times before closing up. This type of behavior is called mode locking. If the rotation number is irrational, the trajectory is quasiperiodic.

The parts of the control parameter space that support periodic behavior are color coded in Fig. 5 up to $q=14$. These regions form Arnol'd tongues [19] that are attached to the curve $\epsilon=\epsilon_1=1$ at $\theta_0/2\pi=p/q$. The two boundaries of the Arnol'd tongues that touch the curve $\epsilon=\epsilon_1=1$ define the locus of saddle-node bifurcations. Tongues show a third boundary "opposite" the contact point on the $\epsilon=1$ axis. This curve is a boundary that defines the beginning of a period-doubling cascade.

The Curry-Yorke map possesses coexisting basins of attraction, in the same way that the van der Pol oscillator exhibits multistability (cf. Figs. 1 and 3). This is shown clearly in Fig. 6. This figure shows the intertwined basins of attraction for coexisting stable period-3 (black) and period-4 (white) orbits for a control parameter value $(\epsilon,\theta_0/2\pi)=(1.7,0.334)$ in the intersection of the period-3 and period-4 windows. Multistability (coexisting basins) is a general feature of overlapping windows in invertible maps.

C. Bifurcation diagrams and phase portraits

In this section we construct two bifurcation diagrams along vertical lines that straddle the point at which the Arnol'd tongue with $p/q=1/3$ intersects the line $\epsilon=1$ in Fig. 5. We choose $\theta_0/2\pi=1/3\pm0.015$. For each bifurcation diagram we also plot the rotation number in the region between the two boundary curves $\epsilon=\epsilon_1$ and $\epsilon_2=f(\theta_0)$.

Figure 7 presents the bifurcation diagram along a path obtained by fixing $\theta_0=2$, so that $\theta_0/2\pi=0.318=1/3-0.015$, varying ϵ, and plotting y_n as a function of ϵ. Also presented in this figure is a plot of rotation number along this path. For $\epsilon\leq1$ there is a fixed point with $y_n=0$. As ϵ increases above 1 the path enters the white region of Fig. 5 above $\theta_0/2\pi=0.318$. This white region describes quasiperiodic behavior. The path enters the Arnol'd tongue that describes the 1/3-locked mode and remains in this tongue for

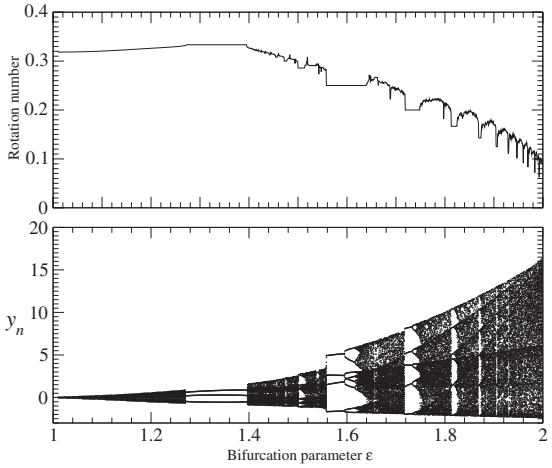

FIG. 7. Bifurcation diagram and rotation number diagram versus ϵ for the Curry-Yorke map. After the Hopf bifurcation, the torus grows in size. Then a period-3 window is observed. It is created and destroyed in saddle-node bifurcations. Other parameter value: $\theta_0/2\pi=2.0/2\pi=1/3-0.015$.

$\epsilon\in[1.273;1.396]$. This is shown by the period-3 window in Fig. 7. On entering this tongue a saddle-node bifurcation creates a stable node and its partner saddle, both of period 3. On leaving this tongue these two orbits self-destruct through an inverse saddle-node bifurcation. The path enters the tongue below the point of intersection with the heteroclinic connection curve and leaves above this point. The sequence quasiperiodicity → mode-locked period 3 → toroidal chaos is observed.

In the range $\epsilon\in[1.396;2.00]$ the path in parameter space enters and leaves many other Arnol'd tongues. In particular, the path transits a number of larger-q tongues before entering a period-4 tongue at $\epsilon\simeq1.56$. The path enters this tongue through its right-hand edge, but leaves through the boundary on the "third side." This boundary separates period-4 behavior from period-8 behavior and indicates the beginning of a period-doubling cascade to chaos. Similar behavior is subsequently seen for period-5 behavior, period-6 behavior, etc. Mode locking is clearly shown in the bifurcation diagram and by the horizontal steps in this devil-like staircase that appears in the rotation number diagram. We point out that the rotation number reaches its maximum value in the period-3 mode-locked window and decreases along this path as the two period-1 regions are approached. At the left edge the rotation number approaches θ_0 as $\epsilon\to\epsilon_1$, and at the right edge the rotation number approaches 0 as $\epsilon\to\epsilon_2$.

Phase portraits of the attractor in phase space along this parameter path are shown in Fig. 8. In the quasiperiodic region for $1.0<\epsilon<1.27$ the trajectory is an ellipse that becomes increasingly deformed as ϵ approaches the 1/3 Arnol'd tongue. Just before reaching the tongue a ghost period-3 orbit makes its presence felt, as indicated in Fig. 8(a). The location of the impending saddle-node bifurcation is indicated by the three large points in this figure. These are responsible for deforming the ellipse into a "triangle." After the saddle-node bifurcation and the metastable quasiperiodic transients have died out, the phase-space portrait is boring: consisting of only three points that remain in place, moving

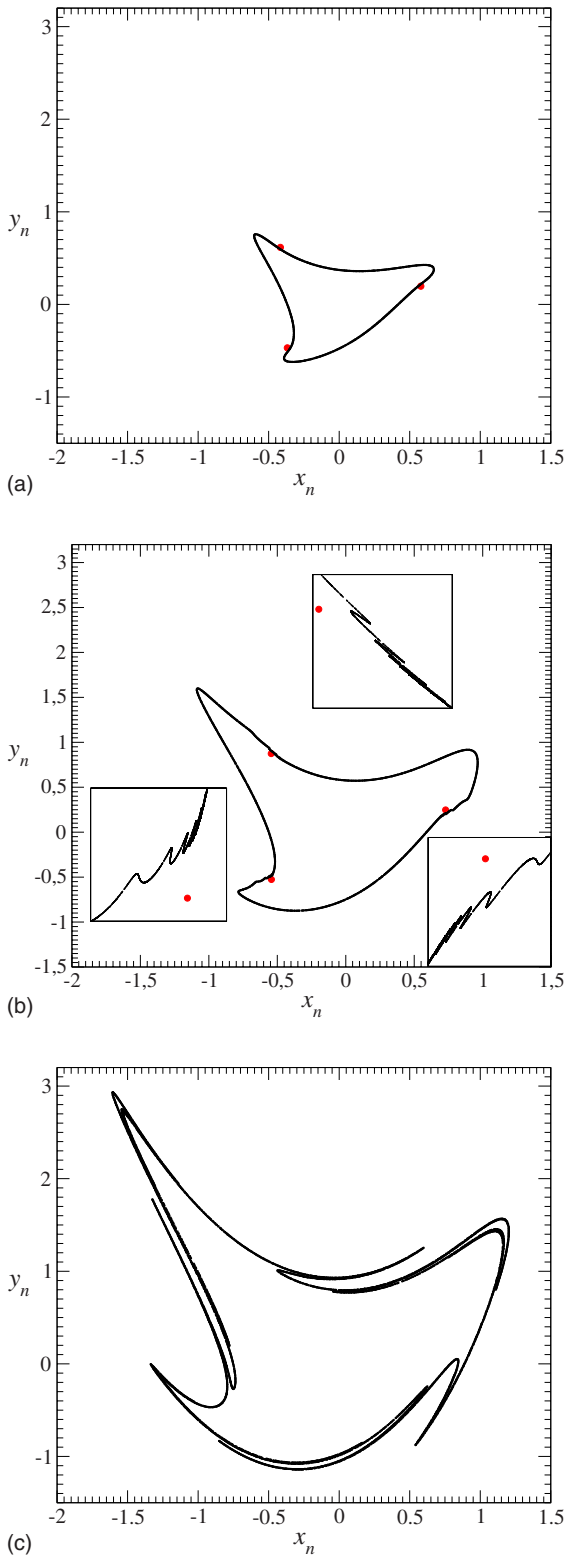

FIG. 8. (Color online) Phase portraits of the Curry-Yorke map along a path with $\theta_0=2/2\pi$. (a) Quasiperiodic behavior along a triangular trajectory just before entering the 1/3 Arnol'd tongue below the heteroclinic tangency point ($\epsilon=1.27$). (b) Toroidal chaotic behavior in a "hard" transition to chaos just after leaving the tongue above the heteroclinic tangency point ($\epsilon=1.40$). (c) Increased folding of the toroidal attractor with increasing nonlinearity ($\epsilon=1.52$). The period-3 points are shown for (a) $\epsilon=1.273$ and (b) $\epsilon=1.39$.

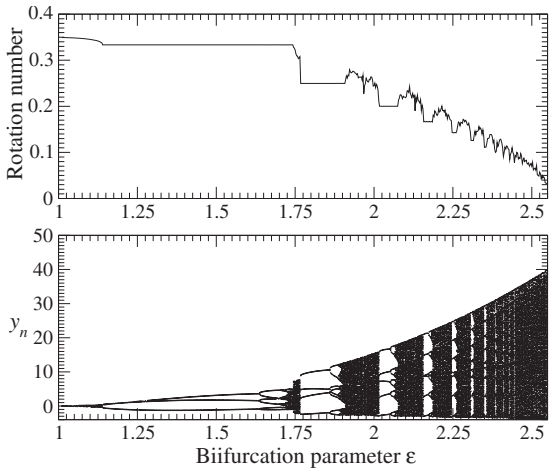

FIG. 9. Bifurcation diagram versus ϵ for the Curry-Yorke map. After the Hopf bifurcation, the torus grows in size. Then a period-3 window is observed before the first foldings occur on the torus. Other parameter value: $\theta_0=\frac{2\pi}{3}+0.1$.

only slightly as the path traverses the Arnol'd tongue. Unseen in this figure is the transition of the path past the heteroclinic tangency curve. The inverse saddle-node bifurcation at $\epsilon=1.396$ leaves a heteroclinic structure that looks like a wrinkled torus as the only local attracting set. It is no longer smooth. This represents a "hard" transition to chaos (cf. Fig. 4 at $\gamma=9.1$). This wrinkled torus is shown in Fig. 8(b) for $\epsilon=1.40$. In this figure we approximate the location of the ghost period-3 orbit by the location of the stable period-3 orbit (circles) for nearby control parameter values. The generally triangular trajectory is now wrinkled, especially in the neighborhood of these phantom fixed points. This is shown clearly in the enlargements in this figure. Temporal evolution of this attracting set exhibits intermittency. As ϵ continues to increase, the attractor becomes increasingly distorted, while it exists. Such increasing distortions are shown in Fig. 8(c) for $\epsilon=1.52$.

We encounter remarkably different behavior by following a path on the other side of the contact point for the mode-locked region with $p/q=1/3$. Figure 9 presents a bifurcation diagram and rotation number diagram obtained by fixing $\theta_0/2\pi=1/3+0.015$. As ϵ increases above 1, the behavior is quasiperiodic with small values of y. The path enters the Arnol'd tongue that describes the 1/3-locked mode, but this time through the right-hand saddle-node boundary and below the heteroclinic curve. The path now exits the period-3 mode-locked region through the "third side" of the Arnol'd tongue. A period-doubling cascade is initiated at $\epsilon\approx1.64$, producing a period-6 limit cycle. The period-doubling cascade reaches the accumulation point at $\epsilon\approx1.722$. For larger values of ϵ chaotic behavior is seen, interrupted by crossings of Arnol'd tongues of the form $1/n$, with $n=4,5,\ldots$. The first tongues encountered exhibit a period-doubling cascade to chaos.

Phase portraits along this path are shown in Fig. 10. Before the period-3 window is encountered the behavior is quasiperiodic with small radius. As the period-3 saddle node bifurcation is approached the quasiperiodic orbit is deformed

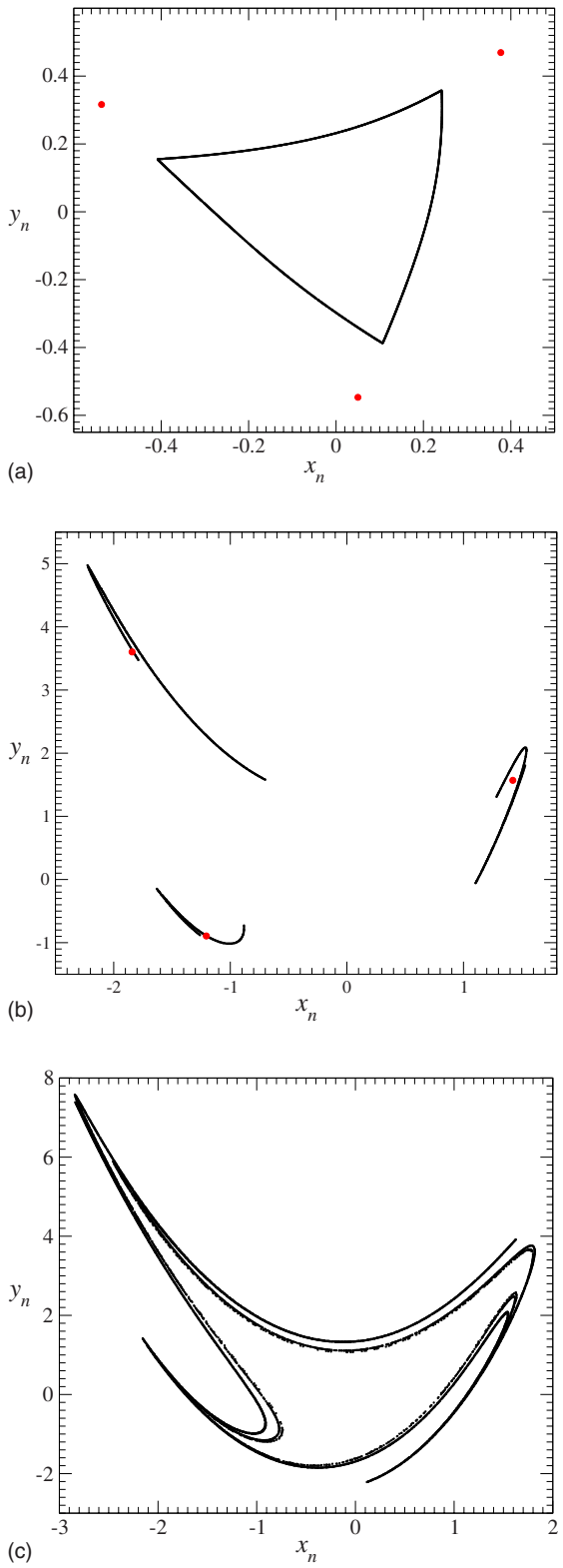

FIG. 10. (Color online) Phase portraits of the Curry-Yorke map along a path with $\theta_0/2\pi=1/3+0.015$. (a) Quasiperiodic behavior along a triangular trajectory just before entering the 1/3 Arnol'd tongue below the heteroclinic tangency point ($\epsilon=1.139$). (b) Banded chaotic attractor after passing out of the period-doubling cascade on the "third side" of the Arnol'd tongue ($\epsilon=1.74$). (c) Chaotic toroidal attractor after a crisis ($\epsilon=1.76$). The period-3 points are shown for (a) $\epsilon=1.140$ and (b) $\epsilon=1.63$.

into the shape of a triangle ($q=3$), shown in Fig. 10(a) along with the ghost saddle-node orbit pair. Beyond the accumulation at $\epsilon\approx 1.722$, there is a unimodal fold in the neighborhood of each ghost period-3 point, shown in Fig. 10(b) [cf. Fig. 2(b)]. This is similar to what is observed after a period-doubling cascade in a Rössler-like system. The chaotic attractor in $\mathbb{R}^3$ can thus be visualized as a chaotic band with three successive stretching-and-squeezing processes. It is only for $\epsilon\approx 1.76$ that a crisis occurs, leading to a bifurcation from a banded chaotic attractor to a toroidal chaotic attractor [Fig. 10(c)]. At this stage, the chaotic attractor is similar to the toroidal chaotic attractor obtained along the curve $\theta_0/2\pi=1/3-0.015$ [compare Fig. 10(c) with Fig. 8(c)]. The attractor becomes increasingly deformed as ϵ continues to increase.

The bifurcation diagram obtained for $\theta_0/2\pi=1/3+0.015$ is roughly similar, beyond the period-3 window, to the bifurcation diagram obtained for $\theta_0/2\pi=1/3-0.015$. The minor differences concern the lengths of the periodic windows, which are slightly larger for the former value of θ_0 because of the shape of the deformed mode-locked region. The rotation number diagram in Fig. 9 shows one difference from that shown for $\epsilon=\frac{1}{3}-0.015$ in Fig. 7. The left-hand edge, at $\epsilon=1$, is the limit on θ_0. For this reason, on approaching the period-3 window, the rotation number rises to $\frac{1}{3}$ in Fig. 7 and decreases to $\frac{1}{3}$ in Fig. 9. In all cases the rotation number approaches zero as the path approaches the upper boundary $\epsilon_2=f(\theta_0)$.

The behavior along paths near other tongues is similar. In the neighborhood of a saddle-node boundary below the heteroclinic intersection the attractor is quasiperiodic and approximates a q-gon for a p/q tongue. Above the heteroclinic intersection the torus is no longer smooth: the invariant set is a toroidal chaotic attractor. Inside a tongue the attractor is a limit cycle of period q.

IV. SUMMARY OF THE TORUS BREAKDOWN THEOREM

Both the van der Pol flow and the Curry-Yorke map satisfy the conditions of the Afraimovich-Shilnikov theorem [4–6]. That is, there exists a smooth invariant torus (an invariant set homeomorphic with a circle for the Curry-Yorke map) for some control parameter values and for others the torus (circle) has been destroyed. When these conditions are satisfied there are three routes to toroidal chaos: by period-doubling bifurcations, by torus wrinkling, and by creation of a homoclinic connection of a saddle cycle.

Mode-locked regions are organized by Arnol'd tongues. Within each tongue there are two curves that describe heteroclinic tangencies between the stable and unstable manifolds of the saddle partner orbit from different sides. These two curves connect the first period-doubling curve within a tongue and each of the two saddle-node boundary curves. The invariant torus exists within the pentagonal-shaped region bounded by these five curve segments. In this region it is structurally stable and dynamically unstable. It breaks down on crossing either of the heteroclinic curves or the first period-doubling curve. A path in control parameter space that leaves a tongue through the "third side" leads, after the

period-doubling cascade, to banded chaotic behavior followed by toroidal chaotic behavior after a series of inverse noisy period-halving bifurcations, as in Fig. 1 at $\gamma=11.0$ and Fig. 10. A path leaving the tongue through a saddle-node edge leads to different types of attractors depending on whether it leaves (a) below or (b) above the intersection point of the heteroclinic curve with the saddle-node curve (shown by $\times$ for the 1/3 tongue in Fig. 5): (a) quasiperiodic behavior if it exits below, as in Fig. 1 at $\gamma=13.9$, or (b) directly to toroidal chaotic behavior in a "hard" transition to chaos, as in Fig. 4 at $\gamma=9.1$ and Fig. 8. Outside a tongue the invariant torus is destroyed when it loses its smoothness with increasing ϵ. This is the "soft" transition to chaos.

The boundaries of a p/q tongue are determined by searching for q doubly degenerate real solutions of the qth iterate of the first return map Eq. (6). Just inside the boundary of a tongue each doubly degenerate solution splits into two nearby nondegenerate real solutions. One q-tuple of solutions describes a stable period-q orbit while the other describes its saddle partner. Just outside the boundary of a tongue each doubly degenerate solution splits into two complex conjugate solutions. These are "ghost" fixed points. They play a significant role in the dynamics. The ghost fixed points are responsible for creating a large invariant density on the attractor in the neighborhood of their real parts, with the density narrowing and increasing as the imaginary part of the solution decreases [20,21].

In the context of the Afraimovitch-Shilnikov theorem, on crossing the saddle-node boundary of an Arnol'd tongue, there is no hysteresis between the attractor inside the tongue (a period-q orbit) and the attractor outside (a quasiperiodic or toroidal chaotic attractor). However, there are remarkable differences in the dynamics. On entering the tongue above the heteroclinic point an initial transient will follow the path of the heteroclinic tangle for a long time before settling down to the stable periodic orbit (metastable chaos). On entering the tongue below the heteroclinic point an initial transient will outline the quasiperiodic attractor that exists just outside the boundary before settling down to the stable periodic orbit (metastable quasiperiodicity). On leaving the tongue above the heteroclinic point an initial condition will evolve in the neighborhood of the ghost period q orbit for a long time before exhibiting chaotic behavior and then returning to nearly periodic behavior (chaotic intermittency [22]). On leaving the tongue below the heteroclinic point the chaotic bursts are replaced by quasiperiodic bursts to account for phase slippage. Intermittency and metastability are opposite sides of the same coin.

The Afraimovich-Shilnikov theorem is local in the sense that it describes torus breakdown associated with a single Arnol'd tongue. It does not deal at all with coexisting attractors, multiple overlapping tongues, and hysteresis. All these features are intrinsic to the van der Pol flow and the Curry-Yorke map. While the Afraimovich-Shilnikov theorem is useful in interpreting the behavior seen in these systems, it does not provide a complete description of these phenomena.

As examples of the additional complexity in these dynamical systems that is not a consequence of this theorem, we point out that hysteresis is clearly shown for the van der Pol oscillator in Fig. 1 and for the Curry-Yorke map in Fig. 11. Multistabilty for the van der Pol oscillator is apparent in Figs. 1–3 and for the Curry-Yorke map in Figs. 5, 6, and 11. Alternation of periodic windows with chaotic behavior is shown in Figs. 1 and 12 for the van der Pol oscillator and in Figs. 7 and 9 for the Curry-Yorke map.

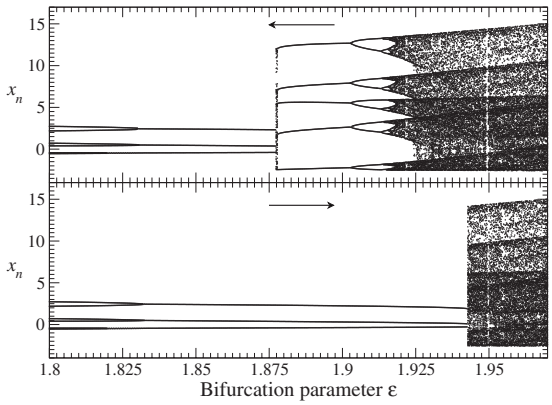

FIG. 11. Bifurcation diagram for the Curry-Yorke map showing hysteresis between the period-3 and period-5 tongues. Compare with Fig. 1 for the van der Pol oscillator. Parameter values: $\theta_0=2.12$ and $\epsilon=1.52$.

V. CONCLUSION

In this paper we showed how the complexity inherent in behavior exhibited by the van der Pol dynamical system can be interpreted in terms of the Curry-Yorke map. We have used this map as a surrogate for the return map of the van der Pol attractor onto a Poincaré surface of section. The correspondence here is not one to one because we have not removed the twofold internal symmetry of the van der Pol attractor by a standard "modding out" process [9]. If this is done, at the cost of making this paper slightly more complicated, the correspondence is yet closer.

When $\epsilon<1$ and $\mu<0$ the return maps exhibit a simple fixed point. As the respective thresholds are crossed, the fixed point becomes unstable and, for $\epsilon-\epsilon_1 \ll 1, \mu \ll 1$, the unstable fixed point is surrounded by a roughly circular trajectory in the plane. As the ratio of the natural to the driving frequency is changed for the van der Pol system or the angle θ_0 is swept in the Curry-Yorke map, this roughly circular trajectory is deformed. As the path in the control parameter space approaches a p/q Arnol'd tongue below the hetero-

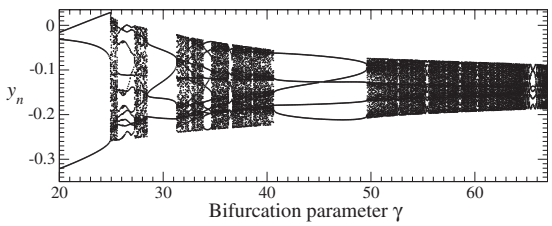

FIG. 12. Bifurcation diagram for the van der Pol oscillator showing alternation of periodic windows and chaotic behavior. Compare with Figs. 7 and 9 for the Curry-Yorke map. Parameter values: $\mu=0.2$, $\omega=1.268$, and $\gamma=8$.

clinic intersection, the quasiperiodic trajectory approaches the shape of a "q-gon" [cf. Figs. 8(a) and 10(a)]. On entering a tongue, the attractor is a stable limit cycle of period q. If the tongue exits through either of the saddle-node edges below the heteroclinic intersection point, the periodic behavior is terminated in a saddle-node bifurcation and the attractor assumes its roughly q-sided shape and quasiperiodic nature. If the path leaves the tongue above the heteroclinic intersection, there is a "hard" transition to toroidal chaos when the period-q limit cycle is destroyed. If the path in the control parameter space exits the tongue through the "third side," a period-doubling cascade begins. If the cascade proceeds past accumulation, a banded chaotic attractor with rotation number p/q will be formed. After a series of noisy period-halving bifurcations, a chaotic toroidal attractor will be formed. On the other hand, if the path reenters the tongue through the "third side," period bubbling will be seen in the bifurcation diagram. Many vertical paths in Fig. 5 exhibit both these types of behavior.

If a path with ϵ in the control space follows a saddle-node edge just outside a p/q Arnol'd tongue, the phase-space trajectory will be a smooth "q-gon" that becomes increasingly deformed and finally loses its smoothness in a "soft" transition from quasiperiodicity to toroidal chaos. The curve defining such transitions can be constructed by "connecting the dots," describing the heteroclinic intersections along the tongues. In regions of overlapping tongues, multistability and hysteresis occur.

[1] C. Hayashi, Y. Ueda, N. Akamatsu et H. Itakura, Trans. Inst. Electron., Inf. Commun. Eng. A **53**, 150 (1970).
[2] Y. Ueda, Nonlinear Sci. Today **2**(2), 1 (1992).
[3] J. H. Curry and J. A. Yorke, Lect. Notes Math. **668**, 48 (1978).
[4] V. S. Afraimovich and L. P. Shilnikov, in *Methods of the Qualitative Theory of Differential Equations* (Izd. Gorkovsk. Gos. Univ., Gorki, 1983), pp. 3–26; Am. Math. Soc. Transl. **149**(2), 201 (1991)
[5] V. S. Anishchenko, M. A. Safonova, and L. O. Chua, IEEE Trans. Circuits Syst., I: Fundam. Theory Appl. **40**, 553 (1993).
[6] M. S. Baptista and I. L. Caldas, Phys. Rev. E **58**, 4413 (1998).
[7] G. M. Zaslavsky, Phys. Lett. **69A**, 145 (1978).
[8] G. M. Zaslavsky and Kh.-R. Ya Rachko, Sov. Phys. JETP **49**, 1039 (1979).
[9] R. Gilmore and C. Letellier, *The Symmetry of Chaos* (Oxford University Press, Oxford, 2007).
[10] O. Menard, C. Letellier, J. Maquet, L. Le Sceller, and G. Gouesbet, Int. J. Bifurcation Chaos Appl. Sci. Eng. **10**, 1795 (2000).
[11] U. Parlitz and W. Lauterborn, Phys. Rev. A **36**, 1428 (1987).
[12] T. Klinger, F. Greiner, A. Rohde, A. Piel, and M. E. Koepke, Phys. Rev. E **52**, 4316 (1995).
[13] A. G. Balanov, N. B. Janson, D. E. Postnov, and P. V. E. McClintock, Phys. Rev. E **65**, 041105 (2002).
[14] A. Algaba, J. Sound Vib. **249**, 899 (2002).
[15] U. Parlitz and W. Lauterborn, Phys. Lett. **107A**, 351 (1985).
[16] U. Parlitz and W. Lauterborn, Z. Naturforsch. Teil A **41A**, 605 (1986).
[17] R. Gilmore and J. W. L. McCallum, Phys. Rev. E **51**, 935 (1995).
[18] L. Achour, Ph.D. thesis, Université de Rouen, 2005.
[19] V. I. Arnol'd, Izv. Akad. Nauk SSSR, Ser. Mat. **25**, 21 (1961); Usp. Mat. Nauk **38**, 189 (1983) [Russ. Math. Surveys **38**, 215 (1983)].
[20] R. Gilmore, *Catastrophe Theory for Scientists and Engineers* (Wiley, New York, 1981).
[21] C. Letellier, P. Werny, J.-M. Malasoma, and R. Gilmore, Phys. Rev. E **66**, 036220 (2002).
[22] P. Manneville and Y. Pomeau, Phys. Lett. **75A**, 1 (1979).